Numer Algor (2018) 79:993–1020
https://doi.org/10.1007/s11075-018-0470-x

ORIGINAL PAPER

Coiflets solutions for Föppl-von Kármán equations governing large deflection of a thin flat plate by a novel wavelet-homotopy approach

Qiang Yu[1] · Hang Xu[1] · Shijun Liao[1]

Received: 7 October 2017 / Accepted: 2 January 2018 / Published online: 11 January 2018

Abstract In this paper, a novel technique incorporated the homotopy analysis method (HAM) with Coiflets is developed to obtain highly accurate solutions of the Föppl-von Kármán equations for large bending deflection. The characteristic scale transformation is introduced to nondimensionalize the governing equations. The results are obtained for the transformed nondimensional equations, which are in very excellent agreement with analytical ones or numerical benchmarks performing good efficiency and validity. Besides, we notice the nonlinearity of the Föppl-von Kármán equations is closely connected with the load and length-width ratio of the plate. For the case of the plate suffering tremendous loads, the traditional linear theory does not work, while our Coiflets solutions are still very accurate. It is expected that our proposed approach not only keeps the outstanding merits of the HAM technique for handling strong nonlinearity, but also improves on the computational efficiency to a great extent.

Keywords Coiflets · Galerkin method · Wavelet · Foppl-von Karman equations

✉ Hang Xu
hangxu@sjtu.edu.cn

[1] Collaborative Innovation Center for Advanced Ship and Deep-Sea Exploration(CISSE), State Key Laboratory of Ocean Engineering, School of Naval Architecture Ocean and Civil Engineering, Shanghai Jiao Tong University, Shanghai 200240, China

1 Introduction

The famous Föppl-von Kármán (FvK) equations governing deflections of a thin flat rectangular plate, proposed by Föppl [1] and von Kármán [2], are written as

$$D\nabla^4 W - h\left(\frac{\partial^2 W}{\partial X^2}\frac{\partial^2 \Psi}{\partial Y^2} + \frac{\partial^2 \Psi}{\partial X^2}\frac{\partial^2 W}{\partial Y^2} - 2\frac{\partial^2 W}{\partial X \partial Y}\frac{\partial^2 \Psi}{\partial X \partial Y}\right) = Q, \tag{1a}$$

$$\nabla^4 \Psi + E\left[\frac{\partial^2 W}{\partial X^2}\frac{\partial^2 W}{\partial Y^2} - \left(\frac{\partial^2 W}{\partial X \partial Y}\right)^2\right] = 0, \tag{1b}$$

where (1a) is derived on basis of kinematic assumptions and the constitutive relations, while (1b) is equivalent to compatibility equation of deformation.

In above equations, $W = W(x, y)$ denotes the vertical deflection, $\Psi = \Psi(x, y)$ is the Airy stress function, h is the thickness of the plate, Q is the vertical external force per unit of area, $D = Eh^3/[12(1-\mu^2)]$ is the bending stiffness of plate, E is the elasticity modulus, μ is the Poisson's ratio ranging from -1 to 0.5, ∇ is the biharmonic operator with the following property

$$\nabla^4 = \nabla^2\nabla^2 = \frac{\partial^4}{\partial X^4} + 2\frac{\partial^4}{\partial X^2 \partial Y^2} + \frac{\partial^4}{\partial Y^4}.$$

Schematic diagram of force analysis and coordinate system is illustrated in Fig. 1, where M_x, M_y are the bending moments, M_{xy} is the torsion moment, Q_x, Q_y are the shear vertical forces, N_x, N_y are the membrane axial forces, N_{xy} is the horizontal shear force, V_x, V_y are the equivalent shear forces. The detailed derivative process are elaborated in literature [3, 4] and can be found in Appendix 1.

Many efforts have been done towards understanding the physical and mathematical mechanism of the Föppl-von Kármán equations by different researchers with various approaches. Among those studies, Knightly [5] obtained a priori bound and

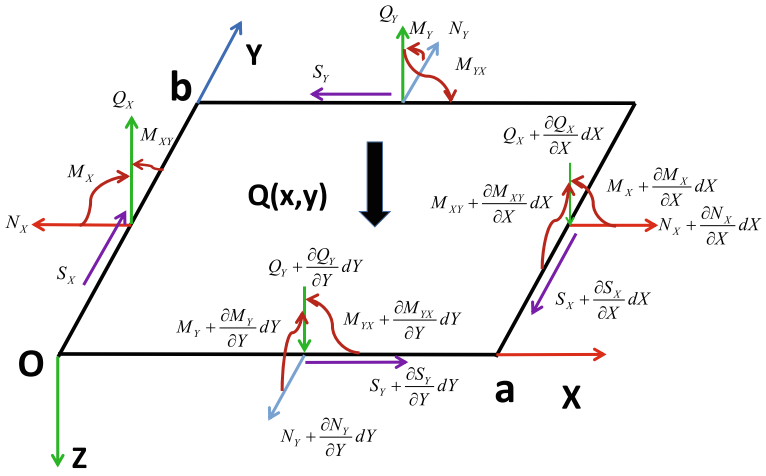

Fig. 1 Force analysis and coordinate system of plate element

a global existence theorem for solutions of the von Kármán equations describing deflections in a thin elastic plate clamped at its edges with combined normal and edge loading being imposed on. Kesavan [6] numerically obtained non-trivial solutions of the Föppl-von Kármán equations using an iterative finite element method which produces approximate solutions bifurcated from a trivial solution close to simple eigenvalues of the linearized problem. Chueshov [7] presented a proof on the existence of wide collection of finite sets of functions for full determination of the long-time solutions of the von Kármán evolution equations and other nonlinear partial differential equations of second order in time. DaSilva and Krauth [8] provided an algorithm that can be used to obtain the solution of the von Kármán's and related problems involving into elasticity theory. By an extraordinary technique of successive reconditioning, their solution took away the convergence difficulties due to various nonlinear stretching and pure bending energies. Lewicka et al. [9] made an extension of the Föppl-von Kármán equations to take account of the shape of stresses in an elastic plate with residual strains, whose formulation was expected to be further applied to describe other active materials in low dimension. Xue et al. [10] applied the von Kármán plate theory on developing a mathematical model on large deflection of a rectangular magnetoelectroelastic thin sheet whose bottom undergoes an acting force due to transverse static mechanical loads. Other typical studies on this topic are found in the papers written by Ciarlet et al. [11, 12], Ciarlet and Gratie [13], Ciarlet and Paumier [14], Ciarlet et al. [15], Milani [16], Coman [17], and Doussouki et al. [18].

Though many numerical and experimental studies with regard to various aspects of the Föppl-von Kármán equations have been done, few researchers have paid their attention to analytical aspects of such equations. Van Gorder [19] firstly made an attempt to obtain analytical solutions of the Föppl-von Kármán equations by combining the HAM technique [20–26]and the Fourier method [27, 28]. He firstly linearized the equations by the HAM technique, by solving a series of linear equations, the analytical approximations are finally obtained for a range of physical parameters. His method has efficiently controlled the item inflation in right part of higher deformation by projecting the solution in functional space spanned by finite trigonometric basis.

In this paper, we develop a novel wavelet-homotopy method to handle the Föppl-von Kármán equations for large bending deflection. In doing so, we introduce the wavelet-Galerkin method into the HAM technique to improve the computation efficiency by choosing Coiflets [29–31] as basis. It should be noted that Xing [32] once tried to combine the HAM technique with wavelet, but his solution was lack of a convergence control parameter, that leads to the convergence of his solution could not be guaranteed. The framework is illustrated as the following. In Section 2, governing equations are dimensionalized and different boundary conditions are put forward. In Section 3, HAM technique is applied to convert the governing equations to a set of linear differential ones. After approximated by wavelets, coupled algebra iterating equations are proposed so as to give Coiflets series. In Section 4, several examples are illustrated to validate solution of our approach. Accurate solutions are given for ultimate load strength in large deformation of plate with fierce nonlinearity.

2 Mathematical formulation

According to the Kirchhoff hypothesis [33], if the plate material is homogeneous and isotropic, then the surface normals remain perpendicular to the neutral plate after deformation. Equations (1a,b) can be formulated via an energy approach with consideration of variations of internal energy and the work done by external forces. Note that membrane displacements and change of plate thickness are negligible.

2.1 The dimensionless equations

The nondimensional Föppl-von Kármán equations derived from (1a,b) are given by

$$\hat{\nabla}^4 w - \left(\frac{\partial^2 w}{\partial x^2}\frac{\partial^2 \varphi}{\partial y^2} + \frac{\partial^2 \varphi}{\partial x^2}\frac{\partial^2 w}{\partial y^2} - 2\frac{\partial^2 w}{\partial x \partial y}\frac{\partial^2 \varphi}{\partial x \partial y}\right) = q, \tag{2a}$$

$$\hat{\nabla}^4 \varphi + K_e\left[\frac{\partial^2 w}{\partial x^2}\frac{\partial^2 w}{\partial y^2} - \left(\frac{\partial^2 w}{\partial x \partial y}\right)^2\right] = 0, \tag{2b}$$

via the following transformations

$$x = \frac{X}{a}, \quad y = \frac{Y}{b}, \quad w = \frac{W}{h}, \quad \varphi = \frac{\Psi h}{D}, \quad \lambda = \frac{b}{a}, \tag{3}$$

where w is the dimensionless vertical deflection, φ is the dimensionless Airy stress function, a, b, and h are, respectively, the length, the width, and the thickness of the plate, dimensionless loads q and constant K_e are

$$K_e = 12(1-\mu^2), \quad q = \frac{K Q a^2 b^2}{E h^4} \tag{4}$$

and the dimensionless biharmonic operator

$$\hat{\nabla}^4 = \lambda^2 \frac{\partial^4}{\partial x^4} + 2\frac{\partial^4}{\partial x^2 \partial y^2} + \frac{1}{\lambda^2}\frac{\partial^4}{\partial y^4}. \tag{5}$$

2.2 Closeness and boundary analysis

In order to ensure (2a,b) being closed while calculation domain $\hat{\Pi} = [0, X] \times [0, Y]$ is transformed to $\Pi = [0, 1] \times [0, 1]$ with the boundary $\Omega = \partial(\Pi)$, 16 boundary conditions have to be taken into consideration. In consideration of an isolated rectangular plate with circled simply supported edge, the bending moment does not exist without external force. In this case, the corresponding boundary conditions in nondimensional forms are written as

$$w(x, y)|_\Omega = \left.\frac{\partial^2 w}{\partial x^2}\right|_{y=0,1} = \left.\frac{\partial^2 w}{\partial y^2}\right|_{x=0,1} = 0, \tag{6}$$

and for circled clamped edge, boundary bending angle is zero without deformation,

$$w(x, y)|_\Omega = \left.\frac{\partial w}{\partial n}\right|_\Omega = 0, \tag{7}$$

and the combined edge that two parallel edges clamped and the other two parallel edge simply supported

$$w(x, y)|_{\Omega} = \left.\frac{\partial w}{\partial x}\right|_{y=0,1} = \left.\frac{\partial^2 w}{\partial y^2}\right|_{x=0,1} = 0. \tag{8}$$

Due to the dimensionless lateral stress meets

$$\sigma_x^m = \frac{1}{K}\frac{\partial^2 \varphi}{\partial x^2}, \quad \sigma_y^m = \frac{1}{K}\frac{\partial^2 \varphi}{\partial y^2}, \quad \tau_{xy} = -\frac{1}{K}\frac{\partial^2 \varphi}{\partial x \partial y} \tag{9}$$

where σ_x^m, σ_y^m are membrane axial stresses and τ_{xy} is membrane shear stress. For an isolate plate, membrane stress circled the plate does not exist which satisfies

$$\left.\frac{\partial^2 \varphi}{\partial x^2}\right|_{y=0,1} = \left.\frac{\partial^2 \varphi}{\partial x \partial y}\right|_{y=0,1} = \left.\frac{\partial^2 \varphi}{\partial y^2}\right|_{x=0,1} = \left.\frac{\partial^2 \varphi}{\partial x \partial y}\right|_{x=0,1} = 0. \tag{10}$$

Except for the boundary conditions due to the surface force distribution, we still need other conditions for $\varphi(x, y)$ to ensure the equations being closed. Without loss of generality, further boundary conditions are supplemented as

$$\varphi(x, 0) = f_1(x), \ \varphi(x, 1) = g_1(x), \ \varphi(0, y) = f_2(y), \ \varphi(1, y) = g_2(y). \tag{11}$$

To let the boundary conditions at edges be compatible, it requires

$$f_1(0) = f_2(0), \quad g_1(1) = g_2(1), \quad f_1(1) = g_2(0), \quad f_2(1) = g_1(0). \tag{12}$$

Regarding physical requirements in (9), which lead to

$$\varphi(x, y) = C_1 x + C_2 y + C_3. \tag{13}$$

It is readily to know that (13) satisfies (2a,b) automatically, which means that C_1, C_2, and C_3 can be any constants. We therefore set $C_1 = C_2 = C_3 = 0$ for convenience. As a result, the following boundary conditions can be given

$$\varphi(x, y)|_{\Omega} = 0. \tag{14}$$

Now, the problem becomes closed and can be solved conveniently.

3 HAM with wavelet basis

In this section, we combine the HAM technique with the wavelet basis to give highly accurate solutions to the above-mentioned problem.

3.1 Linearization by HAM

We first apply the HAM technique to transform the nonlinear equations to a group of linear ones. To do so, we first choose the linear operators as follows:

$$\mathcal{L}_{\varphi} = \mathcal{L}_w = \hat{\nabla}^4. \tag{15}$$

Then, the HAM deformation equations can be constructed as

$$(1-\varrho)\mathcal{L}_w[\Phi(x,y;\varrho)-\Phi(x,y;0)]=\varrho\, c_1 N_w[\Phi(x,y;\varrho),\Theta(x,y;\varrho)], \tag{16a}$$

$$(1-\varrho)\mathcal{L}_\varphi[\Theta(x,y;\varrho)-\Theta(x,y;0)]=\varrho\, c_2 N_\varphi[\Phi(x,y;\varrho),\Theta(x,y;\varrho)], \tag{16b}$$

where $\varrho \in [0,1]$ is an embedding parameter, c_1 and c_2 are the convergence-control parameters, $\Phi(x,y;\varrho)$ and $\Theta(x,y;\varrho)$ are mappings of $w(x,y)$ and $\varphi(x,y)$, $N_w[\Phi,\Theta]$ and $N_\varphi[\Phi,\Theta]$ are nonlinear operators defined by

$$N_w[\Phi,\Theta]=\nabla^4\Phi-\left(\frac{\partial^2\Phi}{\partial x^2}\frac{\partial^2\Theta}{\partial y^2}+\frac{\partial^2\Phi}{\partial y^2}\frac{\partial^2\Theta}{\partial x^2}-2\frac{\partial^2\Phi}{\partial x\partial y}\frac{\partial^2\Theta}{\partial x\partial y}\right)-q, \tag{17a}$$

$$N_\varphi[\Phi,\Theta]=\nabla^4\Theta+K_e\left[\frac{\partial^2\Phi}{\partial x^2}\frac{\partial^2\Phi}{\partial y^2}-\left(\frac{\partial^2\Phi}{\partial x\partial y}\right)^2\right]. \tag{17b}$$

The appropriated boundary conditions are

$$\begin{aligned}
&\Phi(x,0;\varrho)=\frac{\partial^2\Phi(x,0;\varrho)}{\partial x^2}=0, \quad \Phi(x,1;\varrho)=\frac{\partial^2\Phi(x,1;\varrho)}{\partial x^2}=0,\\
&\Phi(0,y;\varrho)=\frac{\partial^2\Phi(0,y;\varrho)}{\partial y^2}=0, \quad \Phi(1,y;\varrho)=\frac{\partial^2\Phi(1,y;\varrho)}{\partial y^2}=0,\\
&\Theta(x,0;\varrho)=\frac{\partial^2\Theta(x,0;\varrho)}{\partial x^2}=0, \quad \Theta(x,1;\varrho)=\frac{\partial^2\Theta(x,1;\varrho)}{\partial x^2}=0,\\
&\Theta(0,y;\varrho)=\frac{\partial^2\Theta(0,y;\varrho)}{\partial y^2}=0, \quad \Theta(1,y;\varrho)=\frac{\partial^2\Theta(1,y;\varrho)}{\partial y^2}=0.
\end{aligned} \tag{18}$$

From (16a,b), we notice

$$\varrho=0, \quad \Phi(x,y;0)=w_0(x,y), \quad \Theta(x,y;0)=\varphi_0(x,y), \tag{19a}$$

$$\varrho=1, \quad \Phi(x,y;1)=w(x,y), \quad \Theta(x,y;1)=\varphi(x,y), \tag{19b}$$

where $w_0(x,y)$ and $\varphi_0(x,y)$ are the initial guesses.

As ϱ increases from 0 to 1, $\Phi(x,y;\varrho)$ and $\Theta(x,y;\varrho)$ vary from their initial guesses $w_0(x,y)$ and $\varphi_0(x,y)$ to the exact solutions $w(x,y)$ and $\varphi(x,y)$. The explicit forms of $\Phi(x,y;\varrho)$ and $\Theta(x,y;\varrho)$ can be expressed by the Taylor expansions with respect to ϱ in the following forms

$$\Phi(x,y;\varrho)=w_0(x,y)+\sum_{M=1}^{+\infty} w_M(x,y)\varrho^M, \tag{20a}$$

$$\Theta(x,y;\varrho)=\varphi_0(x,y)+\sum_{M=1}^{+\infty} \varphi_M(x,y)\varrho^M, \tag{20b}$$

where

$$w_M(x,y)=\frac{1}{M!}\frac{\partial^M\Phi(x,y;\varrho)}{\partial\varrho^M}\bigg|_{\varrho=0}, \tag{21a}$$

$$\varphi_M(x,y)=\frac{1}{M!}\frac{\partial^M\Theta(x,y;\varrho)}{\partial\varrho^M}\bigg|_{\varrho=0}. \tag{21b}$$

The convergent HAM series solutions can be expected as all auxiliary parameters are properly chosen to ensure that the Taylor series all converge at $\varrho = 1$. In this case, we have

$$w(x, y) = w_0(x, y) + \sum_{M=1}^{+\infty} w_M(x, y), \tag{22a}$$

$$\varphi(x, y) = \varphi_0(x, y) + \sum_{M=1}^{+\infty} \varphi_M(x, y). \tag{22b}$$

Differentiating (16a,b) M times with respect to p, then dividing them by $M!$, finally setting $p = 0$, we obtain the Mth-order deformation equations

$$\mathcal{L}_w[w_M - \chi_M w_{M-1}] = c_1\{\nabla^4 w_{M-1} + R_M^w + (\chi_M - 1)q\}, \tag{23a}$$

$$\mathcal{L}_\varphi[\varphi_M - \chi_M \varphi_{M-1}] = c_2\{\nabla^4 \varphi_{M-1} + R_M^\varphi\}, \tag{23b}$$

where

$$R_M^w = -\sum_{s=0}^{M-1}\left(\frac{\partial^2 w_s}{\partial x^2}\frac{\partial^2 \varphi_{M-1-s}}{\partial y^2} + \frac{\partial^2 w_s}{\partial y^2}\frac{\partial^2 \varphi_{M-1-s}}{\partial x^2} - 2\frac{\partial^2 w_s}{\partial x \partial y}\frac{\partial^2 \varphi_{M-1-s}}{\partial x \partial y}\right),$$

$$R_M^\varphi = K_e \sum_{s=0}^{M-1}\left(\frac{\partial^2 w_s}{\partial x^2}\frac{\partial^2 w_{M-1-s}}{\partial y^2} - \frac{\partial^2 w_s}{\partial x \partial y}\frac{\partial^2 w_{M-1-s}}{\partial x \partial y}\right),$$

and

$$\chi_{\bar{k}} = \begin{cases} 0, & \bar{k} \le 1, \\ 1, & \bar{k} > 1. \end{cases} \tag{24}$$

3.2 Coiflets with boundary modification

Solution expressions are very important to improve the convergence of the HAM solutions. However, it is not easy to choose them when the nonlinear problems become considerably complicated. This is due to the solutions of the group of non-homogeneous HAM high-order linear equations can be hardly determined when the solution expressions are not basic functions. To overcome this limitation, we introduce the Generalized Orthogonal Coiflets basis [34] into the HAM technique as the expansion functions.

Due to border jump existence in wavelet, approximate expansions for $f(x)$ at $x = 0$ and $x = 1$ are given by boundary modification of three points interpolation extension in literature [29, 35]

$$\widetilde{f}(x) = \begin{cases} \sum_{k=0}^{3} f\left(\frac{k}{2^j}\right) T_{0,k}(x), x \in (-\delta, 0), \\ f(x), \qquad x \in [0, 1], \\ \sum_{k=0}^{3} f\left(1 - \frac{k}{2^j}\right) T_{1,k}(x), x \in (1, 1+\delta), \end{cases} \tag{25}$$

where δ is small amount, j is resolution level, and $T_{0,k}(x)$ and $T_{1,k}(x)$ are the modification functions defined by

$$T_{0,k}(x) = \sum_{i=0}^{3} \left(\frac{p_{i,k}^{0}}{i!} \right) x^i, \quad T_{1,k}(x) = \sum_{i=0}^{3} \left(\frac{p_{i,k}^{1}}{i!} \right) (x-1)^i \tag{26}$$

with $p_{i,k}^{0}$ and $p_{i,k}^{1}$ determined by coefficient matrices $\mathbf{P_0}$ and $\mathbf{P_1}$.

$$\mathbf{P_0} = \begin{pmatrix} 1 & 0 & 0 & 0 \\ -11/6 & 3 & -3/2 & 1/3 \\ 2 & -5 & 4 & -1 \\ -1 & 3 & -3 & 1 \end{pmatrix}, \quad \mathbf{P_1} = \begin{pmatrix} 1 & 0 & 0 & 0 \\ 11/6 & -3 & 3/2 & -1/3 \\ 2 & -5 & 4 & -1 \\ 1 & -3 & 3 & -1 \end{pmatrix}.$$

Taking the compactly supported $[0, L]$ of wavelets and domain of function $[0, 1]$ into consideration [29], $\widetilde{f}(x)$ is approximated as

$$\widetilde{f}(x) \approx \sum_{k=2-3N}^{2^j-1} \widetilde{f}\left(\frac{M_1 + k}{2^j} \right) \psi(2^j x - k) = \sum_{k=2-3N+M_1}^{2^j-1+M_1} \widetilde{f}\left(\frac{k}{2^j} \right) \psi(2^j x - k + M_1). \tag{27}$$

where M_1 is the first-order vanishing moment, N is the vanishing moment, L is compactly supported length which equals $3N - 1$ in Coiflets family, and ψ is the wavelet basis. It is turned out that coefficients of Coiflets series is the approximate value of the function middle points.

Substitute (25) into wavelet expansion (27), we obtain the desired wavelet basis with boundary modification

$$\phi_{j,k}(x) = \begin{cases} \sum_{i=2-3N+M_1}^{-1} T_{0,k}\left(\frac{i}{2^j} \right) \psi_{j,i}(x) + \psi_{j,k}(x), & k \in [0, 3], \\ \psi_{j,k}(x), & k \in [4, 2^j - 4], \\ \sum_{i=2^j+1}^{2^j-1+M_1} T_{1,2^j-k}\left(\frac{i}{2^j} \right) \psi_{j,i}(x) + \psi_{j,k}(x), & k \in [2^j - 3, 2^j] \end{cases} \tag{28}$$

where

$$\psi_{j,i}(x) = \psi(2^j x - i + M_1), \quad \psi_{j,k}(x) = \psi(2^j x - k + M_1).$$

3.3 Approximation by wavelet basis

In generalized orthogonal Coiflets system [34], resolution wavelet is the same as reconstituted wavelet distinguished from Biorthogonal Coiflets System. Approximation of an arbitrary binary function $G(x, y)$ when $u = v = 0$ and its partial derivatives in x and y directions with u and v orders subjected to homogeneous boundary conditions is

$$\frac{\partial^{u+v}}{\partial x^u \partial y^v} P^j G(x, y) = \sum_{k=0}^{2^j} \sum_{l=0}^{2^j} G\left(\frac{k}{2^j}, \frac{l}{2^j} \right) \phi_{j,k}^{(u)}(x) \phi_{j,l}^{(v)}(y). \tag{29}$$

Moreover, scale of error approximating estimation are conducted in [34] only related to resolution level j, reconstruction level J, vanishing moment and filtering coefficients of wavelets in the following lemma. Besides, some important definitions of mathematical operators are defined in Appendix 2.

Lemma *If arbitrary binary* $G(x, y) \in L^2([0, 1] \times L^2([0, 1]) \bigcap C^N([0, 1] \times [0, 1])$, *the accuracy of the approximation (29) can be estimated as*

$$\left\| \frac{\partial^{u+v} G(x, y)}{\partial x^u \partial y^v} - \frac{\partial^{u+v} P^j G(x, y)}{\partial x^u \partial y^v} \right\|_{L^2} \leq C_p 2^{-j(N-u-v)}, \tag{30}$$

$$\left\| \frac{\partial^{u+v} G(x, y)}{\partial x^u \partial y^v} - \frac{\partial^{u+v} S^J G(x, y)}{\partial x^u \partial y^v} \right\|_{L^2} \leq C_s 2^{-J(N-u-v)}, \tag{31}$$

where C_p *and* C_s *are positive constants that depend only on* $G(x, y)$ *and wavelets, and* $0 \leq u + v < N$.

In view of (6,10,14), boundary matrices $\mathbf{P}_0$ and $\mathbf{P}_1$ are supposed to be modified corresponding to different conditions. For circled simply supported edge, we set

$$\begin{aligned} h^w_{j,k}(x) = h^w_{j,k}(y) = \phi_{j,k}(y)|_{p_{0,2,i}\to 0, p_{1,2,i}\to 0,} \\ h^\varphi_{j,k}(x) = h^\varphi_{j,k}(y) = \phi_{j,k}(y)|_{p_{0,2,i}\to 0, p_{1,2,i}\to 0.} \end{aligned} \tag{32}$$

For circled clamped edge, we set

$$\begin{aligned} h^w_{j,k}(x) = h^w_{j,k}(y) = \phi_{j,k}(y)|_{p_{0,1,i}\to 0, p_{1,1,i}\to 0,} \\ h^\varphi_{j,k}(x) = h^\varphi_{j,k}(y) = \phi_{j,k}(y)|_{p_{0,2,i}\to 0, p_{1,2,i}\to 0,} \end{aligned} \tag{33}$$

and the combined opposite simply supported and fixed edges

$$\begin{aligned} h^w_{j,k}(x) = \phi_{j,k}(x)|_{p_{0,1,i}\to 0, p_{1,1,i}\to 0,}\ h^w_{j,k}(y) = \phi_{j,k}(y)|_{p_{0,2,i}\to 0, p_{1,2,i}\to 0.} \\ h^\varphi_{j,k}(x) = h^\varphi_{j,k}(y) = \phi_{j,k}(y)|_{p_{0,2,i}\to 0, p_{1,2,i}\to 0.} \end{aligned} \tag{34}$$

Later, the dimensionless vertical deflection and the Airy function subjected to homogeneous boundaries are therefore resolved by the Coiflets as

$$w(x, y) \approx P^j w(x, y) = \sum_{k'=1}^{2^j-1} \sum_{l'=1}^{2^j-1} w\left(\frac{k'}{2^j}, \frac{l'}{2^j}\right) h^w_{j,k'}(x) h^w_{j,l'}(y), \tag{35a}$$

$$\varphi(x, y) \approx P^j \varphi(x, y) = \sum_{k'=1}^{2^j-1} \sum_{l'=1}^{2^j-1} \varphi\left(\frac{k'}{2^j}, \frac{l'}{2^j}\right) h^\varphi_{j,k'}(x) h^\varphi_{j,l'}(y). \tag{35b}$$

What needs illustration is that Dirichlet boundary condition decide the scale of coefficients matrices while Neumann type contributes to the modification of boundary matrices $\mathbf{P}_0, \mathbf{P}_1$.

3.4 Algebra iterative equation

According to the general gaussian integration method [30], linear operator $\mathcal{L}$ and nonlinear operator $\mathcal{N}$ acting on approximating function can be transformed on Coiflets basis in the following form

$$\mathcal{R}[\widetilde{f}(x)] \approx \mathcal{R}[P^j \widetilde{f}(x)] = \sum_{k=2-3N+M_1}^{2^j-1+M_1} \widetilde{f}\left(\frac{k}{2^j}\right)\mathcal{R}[\phi_{j,k}(x)] \tag{36}$$

where $\mathcal{R}$ can be replaced by $\mathcal{L}$ or $\mathcal{N}$ to give their corresponding wavelet expressions. Then, we substitute Coiflets expansion of w and φ into Mth order equations

$$\begin{aligned}
&\sum_{k'=1}^{2^j-1}\sum_{l'=1}^{2^j-1}\left\{w_M\left(\frac{k'}{2^j},\frac{l'}{2^j}\right)\mathcal{L}_w[h_{j,k'}h_{j,l'}]\right.\\
&\quad\left. - w_{M-1}\left(\frac{k'}{2^j},\frac{l'}{2^j}\right)\left\{\chi_M\mathcal{L}_w[h_{j,k'}h_{j,l'}] + c_1\hat{\nabla}^4[h_{j,k'}h_{j,l'}]\right\}\right\} \qquad (37)\\
&\quad = -c_1\sum_{k=0}^{2^j}\sum_{l=0}^{2^j}\left[R_M^w\left(\frac{k}{2^j},\frac{l}{2^j}\right) + (1-\chi_M)Q\left(\frac{k}{2^j},\frac{l}{2^j}\right)\right]\phi_{j,k}\phi_{j,l},\\
&\sum_{k'=1}^{2^j-1}\sum_{l'=1}^{2^j-1}\left\{\varphi_M\left(\frac{k'}{2^j},\frac{l'}{2^j}\right)\mathcal{L}_\varphi[\phi_{j,k'}\phi_{j,l'}] - \varphi_{M-1}\left(\frac{k'}{2^j},\frac{l'}{2^j}\right)\left\{\chi_M\mathcal{L}_\varphi[\phi_{j,k'}\phi_{j,l'}]\right.\right.\\
&\left.\left. + c_2\hat{\nabla}^4[\phi_{j,k'}\phi_{j,l'}]\right\}\right\} = -c_2\sum_{k=0}^{2^j}\sum_{l=0}^{2^j}\left[R_M^\varphi\left(\frac{k}{2^j},\frac{l}{2^j}\right)\phi_{j,k}\phi_{j,l}\right]. \qquad (38)
\end{aligned}$$

Finally, by multiplying $\phi_{j,n'}(x)\phi_{j,m'}(y)$ on both ends of (37–38) and integrating on domain Ω, we obtain coupling iterating algebra equations.

$$\hat{\mathbf{W}}_M = (c_1+\chi_M)\hat{\mathbf{W}}_{M-1} + c_1\widetilde{\mathbf{A}}_w^{-1}\widetilde{\mathbf{C}}\bullet\left[\hat{\mathbf{R}}_{M-1}^w + (1-\chi_M)\hat{\mathbf{Q}}\right], \tag{39a}$$

$$\hat{\Phi}_M = (c_2+\chi_M)\hat{\Phi}_{M-1} + c_2K\widetilde{\mathbf{A}}_\varphi^{-1}\widetilde{\mathbf{C}}\bullet\hat{\mathbf{R}}_{M-1}^\varphi, \tag{39b}$$

where straight vectors of variables, nonlinear items and loads are

$$\begin{aligned}
&\hat{\mathbf{F}} = \left\{f_{p'} = f\left(\frac{k'}{2^j},\frac{l'}{2^j}\right)\right\}, \quad f = w_M,\varphi_M, \quad \mathbf{F} = \mathbf{W}_M,\Phi_M,\\
&\hat{\mathbf{F}} = \left\{f_p = f\left(\frac{k}{2^j},\frac{l}{2^j}\right)\right\}, \quad f = R_M^w, R_M^\varphi, q \quad \mathbf{F} = \mathbf{R}_M^w, \mathbf{R}_M^\varphi, \mathbf{Q},\\
&p' = (2^j-1)(k-1)+l,\ o' = (2^j-1)(s-1)+t,\\
&p = 2^jk+l+1, k',l',m',n' = 1\sim 2^j-1, k,l,=0\sim 2^j.
\end{aligned}$$

And the iterating matrices of tensor product

$$\begin{aligned}
&\widetilde{\mathbf{A}}_w^T = \widetilde{\mathbf{A}}_\varphi^T = \lambda^2\Gamma_{k',n'}^{j,4}\bigotimes\Gamma_{l',m'}^{j,0} + 2\Gamma_{k',n'}^{j,2}\bigotimes\Gamma_{l',m'}^{j,2} + \lambda^{-2}\Gamma_{k',n'}^{j,0}\bigotimes\Gamma_{l',m'}^{j,4},\\
&\widetilde{\mathbf{C}}^T = \mathbf{N}_{k,n'}^{j,0}\bigotimes\mathbf{N}_{l,m'}^{j,0}.
\end{aligned}$$

where tensors constructed by connection coefficients

$$\Gamma_{l,m}^{j,n} = \left\{ \gamma_{l,m} = \int_0^1 \frac{d^n h_{j,l}(x)}{dx^n} h_{j,m}(x) dx \right\}, \tag{40}$$

$$\mathbf{N}_{l,m}^{j,n} = \left\{ \bar{\gamma}_{l,m} = \int_0^1 \frac{d^n \phi_{j,l}(x)}{dx^n} h_{j,m}(x) dx \right\}. \tag{41}$$

Straight vectors of nonlinear parts R_M^w, R_M^φ are approximated by products of calculated vectors of w, φ in each order and tensors constituted by Coiflets and its derivatives from (63).

$$\begin{aligned} \hat{\mathbf{R}}_M^w = -\sum_{s=0}^{M-1} \Big[& \hat{\mathbf{W}}_{2,0}^{j,s} \bigodot \hat{\Pi}_{0,2}^{j,M-1-s} + \hat{\mathbf{W}}_{0,2}^{j,s} \bigodot \hat{\Pi}_{2,0}^{j,M-1-s} \\ & - 2\hat{\mathbf{W}}_{1,1}^{j,s} \bigodot \hat{\Pi}_{1,1}^{j,M-1-s} \Big], \end{aligned} \tag{42}$$

$$\hat{\mathbf{R}}_M^\varphi = K_e \sum_{s=0}^{M-1} \left\{ \hat{\mathbf{W}}_{2,0}^{j,s} \bigodot \hat{\mathbf{W}}_{0,2}^{j,M-1-s} - \hat{\mathbf{W}}_{1,1}^{j,s} \bigodot \hat{\mathbf{W}}_{1,1}^{j,M-1-s} \right\}, \tag{43}$$

where the matrices of variables Coiflets expansion are

$$\hat{\mathbf{W}}_{u,v}^{j,M} = (\widetilde{\Phi}_u^j \bigotimes \widetilde{\Phi}_v^j)^T \bullet \hat{\mathbf{W}}_M^U, \quad \hat{\Pi}_{u,v}^{j,M} = (\widetilde{\Phi}_u^j \bigotimes \widetilde{\Phi}_v^j)^T \bullet \hat{\Phi}_M^U, \tag{44}$$

and the coefficients matrices are

$$\hat{\mathbf{W}}_M^U = \left\{ w_p = w_M\left(\frac{k}{2^j}, \frac{l}{2^j}\right) \right\}, \quad \hat{\Phi}_M^U = \left\{ \varphi_p = \varphi_M\left(\frac{k}{2^j}, \frac{l}{2^j}\right) \right\}.$$

4 Results and discussion

In this section, we first make comparison of results obtained from linear equation governed by biharmonic operator in Fourier and Wavelet approach to better understand properties of the Föppl-von Kármán equations. Then, we validate our method by comparing the results with numerical benchmark or analytical one and the computing efficiency in contrast with Gorder's Fourier approach. Besides, nonlinear analysis of large deflection is conducted to study the feasibility of our homotopy-wavelet method.

4.1 Comparison in linear cases

Before solving (23a,b) by the Fourier method, we consider the linear equation governed by biharmonic operator

$$\nabla^4 U(x, y) = \left(\frac{\partial^4}{\partial x^4} + 2\frac{\partial^4}{\partial x^2 \partial y^2} + \frac{\partial^4}{\partial y^4} \right) U(x, y) = T(x, y), \tag{45}$$

which exists a complicated general solution of homogeneous special case by separated variable method

$$U(x, y) = \sum_{\gamma} \sum_{\beta} (C_1 e^{\gamma x} + C_2 e^{-\gamma x})[C_3 \cos(\gamma x) + C_4 \sin(\gamma x)] \times (C_5 e^{\beta y} + C_6 e^{-\beta y})[C_7 \cos(\beta y) + C_8 \sin(\beta y)]. \tag{46}$$

where β, γ are eigenvalue values and the coefficients C_i are determined by the boundary conditions.

As illustrated above, if we solve Mth order deformation equations exactly by determining coefficients, the process will be extremely complicated and very time-consuming. Therefore, the approximate method has to be taken into consideration. In order to study the approximation precision by increasing the series items, we select a particular $T(x, y)$ so that (45) admits an analytical solution $U(x, y)$ (refer to Appendix 2 for the expressions of $T(x, y)$ and $U(x, y)$). It should be pointed out that, for constant $T(x, y)$, the systematic errors on the boundaries are inevitable due to the Gibbs phenomenon when either the Fourier method or the wavelet technique is employed. The analytical solution is extremely difficult to find. As a result, we can hardly illustrate it as the example to check the validity of our solutions. To find an appropriate analytical solution for comparison, we choose such $T(x, y)$ that is combined with polynomial basis.

Besides, we construct the error estimated function $Err(x, y)$ for measuring the error distribution between calculated solution $U^*(x, y)$ and analytical one $U(x, y)$

$$Err(x, y) = |U^*(x, y) - U(x, y)|. \tag{47}$$

Moreover, we define $ErrSQ_1$ and $ErrSQ_2$ as the system error estimated functions, which are written by

$$\begin{aligned} ErrSQ_1 &= ||Err||_{L^1(\mathbf{R})} \approx \frac{1}{M_a M_b} \sum_{k=0}^{M_a} \sum_{l=0}^{M_b} \left| U^*\left(\frac{k}{2^j}, \frac{l}{2^j}\right) - U\left(\frac{k}{2^j}, \frac{l}{2^j}\right) \right|, \\ ErrSQ_2 &= ||Err||_{L^2(\mathbf{R})} \approx \frac{1}{M_a M_b} \sum_{k=0}^{M_a} \sum_{l=0}^{M_b} \left[U^*\left(\frac{k}{2^j}, \frac{l}{2^j}\right) - U\left(\frac{k}{2^j}, \frac{l}{2^j}\right) \right]^2. \end{aligned} \tag{48}$$

where M_a and M_b are numbers of items.

As illustrated in Table 3, by adding items, the approximating precision for both Coiflets and trigonometric approaches can be improved, while the Coiflets is superior than trigonometric ones. On the other hand, using the integral relation (49), it is difficult to determine coefficients of series explicitly, so that it is hard to compute $T(x, y)$ by the Fourier method except that $T(x, y)$ is constant or trigonometric functions. What is pointed in our approach is that polynomial generating recursive integration is introduced, in which the numerical Gauss integral technique is adopted to determine $T(x, y)$.

$$\mathcal{L}^{-1}[T] = \int_0^1 \int_0^1 T(x, y) \sin(m\pi x) \sin(n\pi y) dx dy \tag{49}$$

where m, n are frequency parts.

4.2 Validation and comparison in nonlinear case

In this case, our proposed technique is employed to solve the nonlinear equations (2a) and (2b). Here, the indicators of measuring errors are defined as

$$Err_f = \frac{1}{(2^j+1)^2}\sum_{k=0}^{2^j}\sum_{l=0}^{2^j}\left[f_M\left(\frac{k}{2^j},\frac{l}{2^j}\right)\right]^2, \quad f = w, \varphi \tag{50}$$

$$ErrSQ_f = \frac{1}{(2^j+1)^2}\sum_{k=0}^{2^j}\sum_{l=0}^{2^j}\left[f\left(\frac{k}{2^j},\frac{l}{2^j}\right) - f^*\left(\frac{k}{2^j},\frac{l}{2^j}\right)\right]^2, \quad f = w, \varphi \tag{51}$$

where $f(x, y)$ and $f^*(x, y)$ are the homotopy-wavelet and the analytical solutions, respectively. Note that the convergent result is expected when Err_f tends to zero. Note also that the diminishment of the residual (51) indicates that our solutions approach to the analytical ones. Our code is based on the software Mathematica ver.10 and can be readily run on a personal computer with an Intel Core 4 Quad 2.5 GHz CPU and 8GB memory.

4.2.1 Validation in different boundary conditions

We first validate our approach in comparison with numerical benchmark. Dimensionless deflection, bending and membrane stresses distributions at $x = 1/2$ of plate subjected to circled simply supported movable edge(CSSME) or circled clamped movable edge(CCME) suffering load $q = 128K_e, 192K_e$ respectively by Analog Equation Method (AEM) were given by Katsikadelis and Nerantzaki [36]. In contrast to values by our approach in resolution $j = 5$, three figures show an excellent agreement in Figs. 2, 3, and 4. On the whole, it is obvious that bearing load capacity of plate

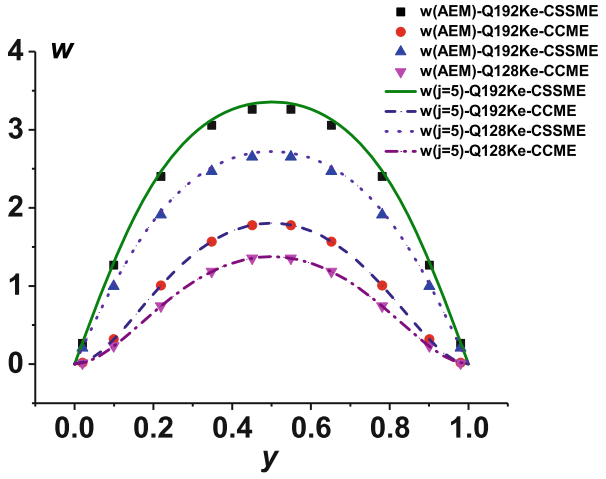

Fig. 2 Dimensionless deflection w comparison for boundaries of circled simply supported movable edge (CSSME) or circled clamped movable edge (CCME). Line: Analog Equation Method(AEM), Point: wHAM at resolution level $j = 5$

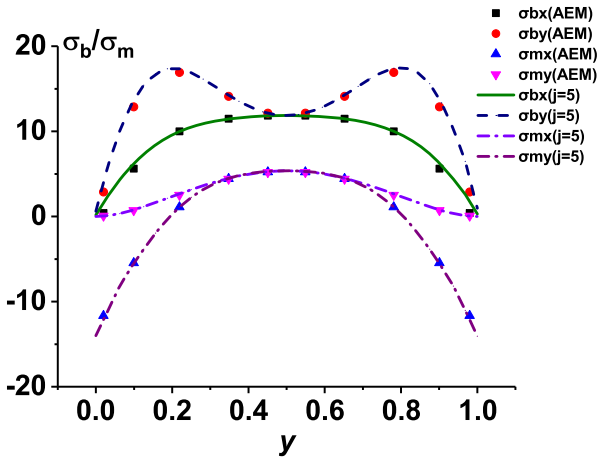

Fig. 3 Bending and membrane stresses comparison subjected to circled simply supported movable edge (CSSME) when $q = 128K_e$. Line: Analog Equation Method (AEM), Point: wHAM at resolution level $j = 5$

subjected to clamped edge is better than that subjected to simply supported edge. Besides, in Table 1, with the resolution level j increases, obtained central maximum deflection is more and more near classical exact one. In comparison of results by Azizian [37] and Wang [38] using Finite Strip and DRBEM, the absolute errors when $q = 10, 50, 75, 100$ is around order 10^{-3} while the other two methods are around 10^{-2}. Therefore, in this case, the accuracy of our method is much better. As illustrated in Table 2, compare to results by Al-Tholaia [39] using RBF meshless method and finite element method (FEM), we figure out convergent deflection and stress of plate subjected to CSSME suffering $q = 40$ in resolution level $j = 3 \sim 6$, which

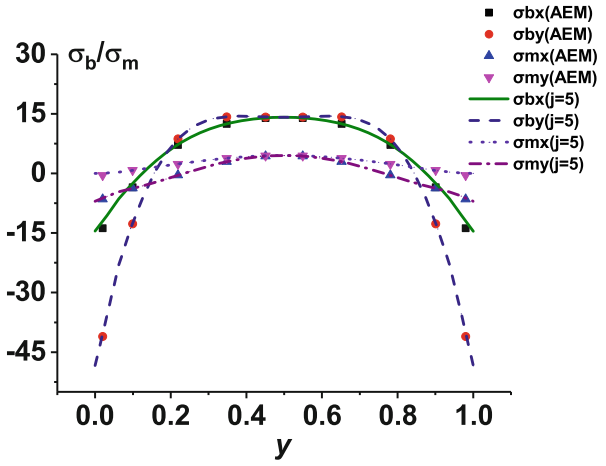

Fig. 4 Bending and membrane stresses comparison subjected to circled clamped movable edge (CCME) when $q = 192K_e$. Line: Analog Equation Method(AEM), Point: wHAM at resolution level $j = 5$

Table 1 Dimensionless deflection comparison between AEM and our approach with different loads($c_1 = c_2 = -3/5, iter = 5, M = 10$)

q	10	50	75	100
Classic [37]	0.019149	0.095147	0.14155	0.18671
Azizian [37]	0.019908	0.098833	0.14694	0.19361
Wang [38]	0.0196312	0.0980101	0.146729	0.195117
This work($j = 3$)	0.0204734	0.102218	0.146529	0.203523
This work($j = 4$)	0.019598	0.0978571	0.146529	0.1949
This work($j = 5$)	0.0192927	0.0963329	0.144247	0.191864
This work($j = 6$)	0.0192125	0.0959326	0.143648	0.191068
Relative error (Azizian)	3.96E-02	3.87E-02	3.81E-02	3.70E-02
Relative error (Wang)	2.52E-02	3.01E-02	3.66E-02	4.50E-02
Relative error ($j = 6$)	3.32E-03	8.26E-03	1.48E-02	2.33E-02

also performs excellent agreement by iterating HAM [40] that iteration ($iter = 5$) and order ($M = 10$), as shown in Table 3.

We then construct general equations containing exact solutions by adding item p in right side of (2b) while the Föppl-von Kármán equations are the special case. By setting $c_1 = -92/100$ and $c_2 = -88/100$, and choosing $\lambda = 1$ and $K_e = 9/100$, we first illustrate our Coiflets solutions with $q(x, y)$ and $p(x, y)$ being given in Appendix 2.

As illustrated thereinafter, our reconstituted solutions agree well with the analytical solutions, which show the validity of our proposed approach. Particularly, we notice that the reconstituted Coiflets solutions (35a,b) are very accurate since the Coiflets is compactly supported by performing finite regularity that are not infinitely differentiable. As shown in Fig. 5a, the norms of w at $j = 6$ decrease to 10^{-4} by 15 iterations and 10^{-10} by 40 iterations. The convergent rate can be adjusted by altering c_1 and c_2. Moreover, as showed in Table 4, the system residual errors of w and φ diminish rapidly to 10^{-7} for the resolution level $j = 6$.

Since limited precision for calculation of the connection coefficients based on the filtering coefficients of Coiflets is selected to simplify calculation, the residual

Table 2 Comparison of dimensionless deflection w, bending stress σ_b and membrane stresses σ_m between RBF, FEM, and our approach($c_1 = c_2 = -1/4, iter = 5, M = 10$)

Methods	w	σ_b	σ_m	Time (s)
This work ($j = 3$)	1.53952	10.1476	1.5734	0.3637574
This work ($j = 4$)	1.40467	8.06868	1.70394	3.1362198
This work ($j = 5$)	1.36063	7.88887	1.65281	31.7269536
This work ($j = 6$)	1.35013	7.84265	1.63751	385.4753171
RBF [39]	1.3619	7.7815	1.6611	–
FEM [41]	1.3508	7.6551	1.6359	–

Table 3 Approaching precision and consuming time by Fourier and Wavelet approach with different number of items in linear case

Item number	9×9	17×17	33×33	65×65
Fourier-ErrSQ$_1$	5.07E-02	3.97E-02	3.55E-02	3.37E-02
Fourier-ErrSQ$_2$	2.94E-02	1.16E-02	4.99E-03	2.26E-03
Wavelet-ErrSQ$_1$	2.52E-01	6.70E-02	6.98E-03	5.17E-04
Wavelet-ErrSQ$_2$	1.70E-01	4.38E-02	4.49E-03	3.33E-04
Fourier-Time (s)	2.24E+02	1.40E+03	4.25E+03	3.85E+04
Wavelet-Time (s)	7.66E-01	1.09E+00	3.22E+00	3.58E+01

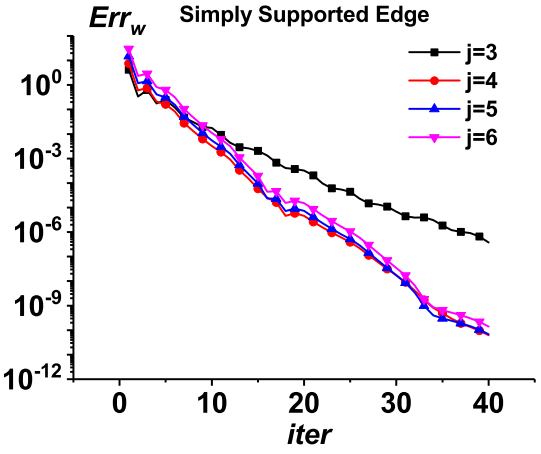

(a) Err_w.

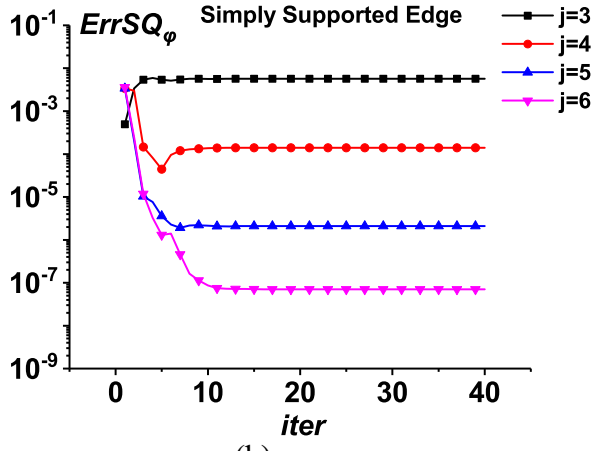

(b) $ErrSQ_w$.

Fig. 5 **a**, **b** Norm of Mth order solution and residual vary with iteration subjected to circled simply supported boundary. Square: $j = 3$; circle: $j = 4$; delta: $j = 5$; nabla: $j = 6$

Table 4 Convergent results of order $M = 15$ in different resolution level j subjected to simply supported boundary

j	3	4	5	6
Item number	9×9	17×17	33×33	65×65
Err_w	2.07E-03	5.88E-05	9.54E-05	1.96E-04
Err_φ	4.73E-04	5.10E-05	8.23E-05	1.68E-04
ErrSQ_w	8.71E-03	1.40E-04	2.33E-06	8.35E-08
ErrSQ_φ	5.69E-03	1.19E-04	2.10E-06	7.10E-08
Time (s)	1.90E-02	8.33E-01	1.83E+01	2.53E+02

errors are reduced to a certain order of magnitude that is a straight line, as illustrated in Fig. 5b. Due to this reason, too many iterations in our approach are unnecessary. Particularly, by increasing the resolution level, the approaching precision can be improved but the computing process becomes more time-consuming. Therefore, by choosing an appropriate convergent precision corresponding to a prescribed j, we are able to achieve our target effectively using our proposed approach.

Further, to validate the generality of our technique for adapting other kinds of boundary conditions, the large deflection plate subjected to the circled rigid fixed and combined boundaries is considered; the parameters for this problem are defined in Appendix 2. By setting proper convergence control parameters and modifying difference coefficient matrices, in the case of $\lambda = 1$ and $K_e = 9/100$, our results are also in accordance with the analytical ones, as illustrated hereinafter. From Tables 5 and 6, the solutions of w and φ are successfully given with high precision and efficiency. The residuals decrease into order of magnitude around 10^{-4}, 10^{-6}, and 10^{-8} at the resolution level $j = 4, 5$ and 6 within nearly $0.74s$, $17.3s$, and $268.69s$, respectively. Moreover, the comparison of deformation in middle line $x = 0.5$ with the analytical solution and the absolute errors is presented in Fig. 6. It is seen that the deflection results are in coincidence with the exact ones, the absolute average errors are in the level of $10^{-4.5}$, 10^{-3}, and $10^{-3.2}$ corresponding to the three different boundaries.

Table 5 Convergent results of order $M = 15$ in different resolution level j subjected to clamped edge

j	3	4	5	6
Item number	9×9	17×17	33×33	65×65
Err_w	1.71E-03	3.43E-05	2.72E-05	5.06E-05
Err_φ	2.49E-04	1.49E-05	2.11E-05	4.11E-05
ErrSQ_w	7.95E-03	4.95E-05	2.13E-06	2.04E-08
ErrSQ_φ	9.59E-03	1.91E-04	2.71E-06	7.27E-08
Time (s)	1.90E-02	7.41E-01	1.73E+01	2.69E+02

Table 6 Convergent results of order $M = 15$ in different resolution level j subjected to combined boundary

j	3	4	5	6
Item number	9×9	17×17	33×33	65×65
Err_w	2.91E-03	2.61E-04	3.86E-04	7.67E-04
Err_φ	2.37E-04	4.51E-05	7.27E-05	1.45E-04
ErrSQ_w	9.87E-04	5.13E-06	4.96E-08	5.05E-08
ErrSQ_φ	4.99E-03	1.13E-04	2.02E-06	7.07E-08
Time (s)	2.05E-02	7.46E-01	1.72E+01	2.67E+02

4.2.2 Comparison with the fourier approach

Here, we revisit Gorder's problem [19] by the Fourier approach. The solution series for Mth orders in nondimensional form are

$$w(x,y) \approx \frac{4}{\pi^4} \sum_{k=0}^{M} \sum_{m=1}^{M_w} \sum_{n=1}^{N_w} \frac{w_{m,n}^{[k]} \sin(m\pi x) \sin(n\pi x)}{(\lambda m^2 + \lambda^{-1} n^2)^2}, \tag{52a}$$

$$\varphi(x,y) \approx \frac{4}{\pi^4} \sum_{k=0}^{M} \sum_{m=1}^{M_\varphi} \sum_{n=1}^{N_\varphi} \frac{\varphi_{m,n}^{[k]} \sin(m\pi x) \sin(n\pi x)}{(\lambda m^2 + \lambda^{-1} n^2)^2}, \tag{52b}$$

where M_w, N_w and M_φ, N_φ are number of items.

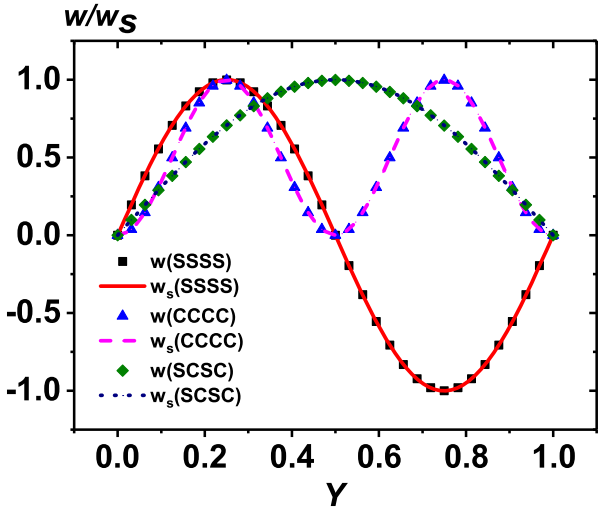

Fig. 6 Comparison of calculated deformation with analytical one at $x = 1/2$ subjected to different boundary conditions. Line: analytical solution; scatter: calculated solution. Solid and square: circled simply supported edge(SSSS); dash and up triangle: circled clamped edge(CCCC); dot and diamond: combined edge (SCSC)

As shown in Table 7, both the errors $ErrSQ_w$ and $ErrSQ_\psi$ decrease as the valid number of series terms increase. The computational time increases as more terms involve. Here, the valid terms denote the odd coefficients of the series expansions, which have relationships $M_w = N_w = 2m - 1$ and $M_\varphi = N_\varphi = 2n - 1$. Using the software *Mathematica*, the complex integral operation is simplified to a set of trigonometric product terms that can be readily used for summation and algebra operation.

In general, increase of number of the series items can improve the accuracies of both methods, but the approximating precision of our homotopy-wavelet approach is better than the Fourier method if the same number of series items is chosen. From Tables 4 and 7, we know that the results by 8×8 trigonometric basis are equivalent to those ones by the Coiflets at $j = 3$. In both cases, the errors of w, φ are in level of 10^{-3} . To achieve such accuracies, Fourier method consume 846.59 s, but our proposed approach only needs 0.02 s. We only need a few iterations to achieve accurate results whose errors can reduce to 10^{-6} and 10^{-8} with 32×32 and 64×64 at $j = 5$ and $j = 6$ within 18.27 and 253.33 s, respectively. Particular attention should be paid for lower order computation, which is usually hard to give solutions with high precision. As a result, the high-order computation is often employed to improve on the computational accuracies. To avoid wasting computational time, iterating HAM technique is used in the calculation.

Essentially, there are several differences between the two approaches. Firstly, different ways for handling boundary conditions. In Fourier method, the boundary conditions are automatically satisfied by the proper choice of the solution expressions and initial guesses. While in wavelet technique, the boundary polynomial interpolation extension is adopt to avoid the secular term and the computational precision loss. Secondly, different techniques for handling nonlinear parts. In Fourier method, the nonlinear parts are expanded as the summation of a series of functions which grow exponentially as the computational order increases. Nevertheless, in wavelet approach, the nonlinear parts are considered as a whole function to be approached by

Table 7 Results of HAM by Fourier approach with iteration subjected to simply supported boundary

Valid items	3×3	4×4	5×5	6×6
$M_w, N_w, M_\varphi, N_\varphi$	5	7	9	11
(M,iteration)	(10,1)	(10,1)	(8,1)	(8,1)
ErrSQ$_w$	2.41E-02	1.93E-02	1.52E-02	1.29E-02
ErrSQ$_\varphi$	1.40E-01	8.32E-02	4.13E-02	2.69E-02
Time (s)	1.58E+01	3.21E+01	6.63E+01	1.76E+02
Valid items	7×7	8×8	9×9	10×10
$M_w, N_w, M_\varphi, N_\varphi$	13	15	17	19
(M,iteration)	(5,1)	(4,2)	(3,3)	(2,5)
ErrSQ$_w$	8.12E-03	4.12E-03	2.08E-03	1.36E-03
ErrSQ$_\varphi$	1.22E-02	7.15E-03	4.19E-03	2.98E-03
Time (s)	4.16E+02	8.46E+02	1.53E+03	2.72E+03

wavelet basis, which greatly decreases the computational complexity. Thirdly, different way for controlling precision of solutions. In Fourier method, the effective way to improve on the solution precision is to involve more terms into the computation, which are very time-consuming. In wavelet approach, the precision is only related to resolution level j without considering approximating functions. Once j is given, the projecting function space scale and the number of items are determined in the meantime. It is very convenient to obtain the reconstitution solution with certain accuracies if the convergence control parameters are properly chosen.

4.3 Nonlinearity analysis and application

When a flat plate suffers small deflection ($w/h \leq 0.2$), the film stress can be neglected compared to the bending stress. The latter dominates the deformation due to $\sigma_x^m = \sigma_y^m = \tau_{xy}^m = 0$ which leads $\varphi \approx 0$.

Equations (1a) and (b) are simplified as $D\nabla^4 W = Q$ using the Fourier way. The dimensionless maximum deflection on plate is nearly proportional to the load q, while k_1 is supposed to be constant due to the uniform distribution of the load. With those assumptions, the following relationship can be obtained

$$w_{\max} = \frac{W_{\max}}{h} = k_1 \frac{Qa^2b^2}{Eh^4} = \frac{k_1}{K} q. \tag{53}$$

It is obviously that the nonlinear part of (2a) and (b) are determined by K_e which is related to the Poisson's ratio μ, the length-width ratio λ, and the dimensionless loads q. In order to study their relations, we set q/K_e as a variable for calculating the large deformation with different λ. For the sake of comparison, we also use the linear theory to give solutions. Parameters of the rectangular plate are chosen as $\mu = 0.3$, $E = 2.06 \times 10^{11} N/m^2$, the thickness $h = 18$mm, the length $a = 1$m with length-width ratio being $\lambda = 1, 2, 3, 5$ subjected to circled simply supported edge.

As illustrated before, our proposed approach is able to obtain highly accurate solutions with strong nonlinearity by choosing appropriately convergence control parameters. Here, we need to make more assumptions to let the problem be physically realistic. (1) The loads on the plate is finite. (2) The surface bending is within the elastic range. The ultimate dimensionless loads q are discussed based on these assumptions.

The influence of q/K_e on the dimensionless deflection W/h is shown in Fig. 7. Both the linear and the nonlinear results are given, respectively, by the linear theory and by our proposed technique. It is found from the figure that when q/K_e is small, corresponding to the weak nonlinearity case, the results give by two techniques are quite similar. This indicates that linear theory can work well for small q/K_e. While as q/K_e is large, corresponding to the stronger nonlinear case, the results are markedly different, the linear result is obvious beyond the nonlinear result. The linear theory is obviously not applicable in such situation. Particularly, if we keep the convergence-controlled parameters unchanged, there is a maximum q/K_e, beyond this value, the solution is divergent. The ultimate q/K_e respectively approximates 27.74, 36.99, 41.62, and 57.80 for $\lambda = 1, 2, 3, 5$ by setting $c_1 = c_2 = -0.9$. To give accurate results beyond this maximum q/K_e, the convergence-controlled parameters

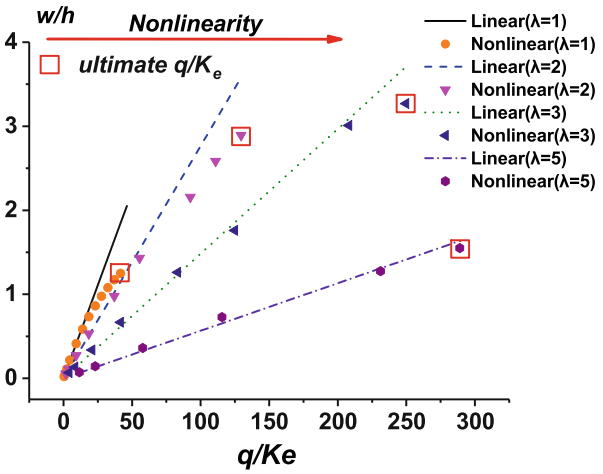

Fig. 7 Dimensionless calculated deflection W/h vary with q/K_e by linear theory and wavelet approach in different length-width ratio λ. Solid line, linear results $\lambda = 1$; dash line, linear results $\lambda = 2$; dot line, linear results $\lambda = 3$; dot line, linear results $\lambda = 3$; circle, nonlinear results $\lambda = 1$; down triangle , nonlinear results $\lambda = 2$; left triangle, nonlinear results $\lambda = 3$; hexagon, nonlinear results $\lambda = 5$

have to be altered accordingly. As the nonlinearity become strong, it is more difficult to give accurate solutions. In this situation, we can adjust the values of the convergent-controlled parameter to ensure our solution being convergent. As shown in Fig. 8, by altering the convergent-controlled parameters c_1, c_2 from -1 to 0, the maximum value of q/K_e can be enlarged to around 46.24, 129.48, 208.09, and 289.02 for $\lambda = 1, 2, 3, 5$, respectively. For example, in comparison with benchmark by RBF method [39], $q/K_e = 40$ corresponds to dimensionless deflection $w = 1.36$ while $w = 1.35546$ by our approach and 2.05136 by linear theory.

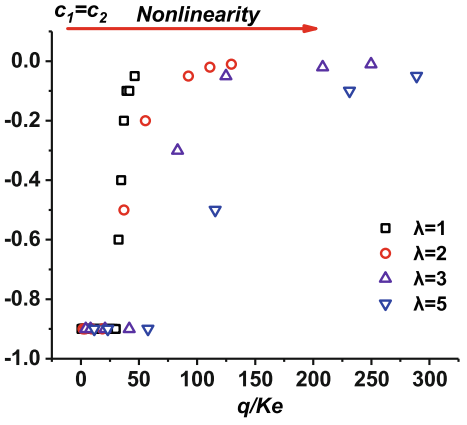

Fig. 8 Optimal convergence control parameter c_1 vary with q/K_e in different length-width ratio λ. Square: $\lambda = 1$; circle: $\lambda = 2$; up triangle: $\lambda = 3$; down triangle: $\lambda = 5$

From our computation, we also notice that the length-width ratio λ is an important factor to affect the nonlinearity of the governing equations. When λ is small, the nonlinearity is strong. The difference of solutions between the linear theory and our proposed method is clear. when λ increases, the nonlinearity becomes weak, the solutions obtained by two approaches have no evident difference. This indicates that increase of λ is helpful to improve on the maximum q. On the other hand, if the plate suffers the same load, the larger λ generates smaller deformation. This is the reason why 2D cylinder bending plate with large length-width ratio can be transformed into 1D one by lath bean theory.

5 Conclusion

In this paper, we present a novel technique that combines the HAM technique and the wavelet basis to obtain highly accurate solutions of partial differential equations with strong nonlinearity. Nonlinear equations are transformed into a set of infinite linear ones by selecting proper convergence-controlled parameters. Then, by the wavelet-Galerkin method, the high-order deformation equations are solved using the Coiflets basis. The process is to transform linear differential equations into linear algebra ones in certain approximation accuracy decided by the vanishing moment and the resolution level. The Föppl-von Kármán equations are used as an example to illustrate the validity and efficiency of our proposed technique. Dimension analysis of the Föppl-von Kármán equations is conducted, which shows that the nonlinearity of dimensionless ones is related to dimensionless loads q, length-width ratio λ, and materials decided by μ. Linear equation governed by biharmonic operator and nonlinear Föppl-von Kármán equations are considered as a comparative example. Results reveal that the linear theory is only valid for the weak nonlinear case, while our proposed technique is valid for both the weak and strong nonlinear cases. In summary, the following conclusions can be reached:

1. The Coiflets wavelet basis is introduced into HAM technique. The novel technique is fit for strong nonlinear problems with better computational efficiency.
2. The series items are fixed in this technique for solving the high-order deformation equations, which is totally different from the traditional HAM technique. The computational accuracy is only related to the resolution level when the approaching function space is finite. The essence is to obtain projection in function space spanned by Coiflets, which sacrifices systemic errors between projection and analytical solutions to improve computational efficiency.
3. This approach is suitable for various homogenous boundary conditions concerning simply supported, clamped, and combined ones while reconstituted solutions are in agreement with analytical or numerical ones.
4. With the assumptions that the Kirchhoff hypothesis of surface bending is valid and within the elastic range, the linearized equation is only effective on a certain accuracy denoting plate under weak loads. While our approach has powerful ability and high computing efficiency to obtain convergent solutions for large deflection without linearization.

Funding information This work is partially supported by the National Natural Science Foundation of China (Approval No. 11272209 and 11432009).

Appendix 1: Derivative process of governing equations

In classic elastic mechanics, U, V, and W denote displacement of mass point on plate. Thus, the relationship between strain and displacement by neglecting all other higher order terms can be written as

$$\varepsilon_X^m = \frac{\partial U}{\partial X} + \frac{1}{2}\left(\frac{\partial W}{\partial X}\right)^2 \quad \varepsilon_X^b = -Z\frac{\partial^2 W}{\partial X^2}, \tag{54a}$$

$$\varepsilon_Y^m = \frac{\partial V}{\partial Y} + \frac{1}{2}\left(\frac{\partial W}{\partial Y}\right)^2 \quad \varepsilon_Y^b = -Z\frac{\partial^2 W}{\partial Y^2}, \tag{54b}$$

$$\gamma_{XY}^m = \frac{\partial U}{\partial Y} + \frac{\partial V}{\partial X} + \frac{\partial W}{\partial X}\frac{\partial W}{\partial Y} \quad \gamma_{XY}^b = -2Z\frac{\partial^2 W}{\partial X \partial Y}, \tag{54c}$$

where ε is the normal strain, γ is the shearing strain, the superscript m and b means that the strains are the film strain and the bending strain respectively while total strain is the sum

$$\varepsilon_X = \varepsilon_X^m + \varepsilon_X^b, \tag{55a}$$

$$\varepsilon_Y = \varepsilon_Y^m + \varepsilon_Y^b, \tag{55b}$$

$$\gamma_{XY} = \gamma_{XY}^m + \gamma_{XY}^b. \tag{55c}$$

Eliminating the bending strain from above equations, we obtain

$$\frac{\partial^2 \varepsilon_X^m}{\partial X^2} + \frac{\partial^2 \varepsilon_Y^m}{\partial Y^2} - \frac{\partial^2 \gamma_{XY}^m}{\partial X \partial Y} = \left(\frac{\partial^2 W}{\partial X \partial Y}\right)^2 - \frac{\partial^2 W}{\partial X^2}\frac{\partial^2 W}{\partial Y^2}. \tag{56}$$

Based on the Hooke law, the bending and film stress are written as

$$\sigma_X = \sigma_X^m + \sigma_X^b = \frac{E}{1-\mu^2}(\varepsilon_X + \mu\varepsilon_Y), \tag{57a}$$

$$\sigma_Y = \sigma_Y^m + \sigma_Y^b = \frac{E}{1-\mu^2}(\varepsilon_Y + \mu\varepsilon_X), \tag{57b}$$

$$\tau_{XY} = \tau_{YX} = \tau_{XY}^m + \tau_{XY}^b = \frac{E}{2(1+\mu)}\gamma_{XY}. \tag{57c}$$

Assuming that the plate is homogeneous, the bending moments M_X, M_Y and shear moment M_{XY} are obtained, by integrating stress along the thickness direction, as

$$M_X = \int_{-h/2}^{h/2} \sigma_X Z dZ = -D\left(\frac{\partial^2 W}{\partial X^2} + \mu\frac{\partial^2 W}{\partial Y^2}\right), \tag{58a}$$

$$M_Y = \int_{-h/2}^{h/2} \sigma_Y Z dZ = -D\left(\frac{\partial^2 W}{\partial Y^2} + \mu\frac{\partial^2 W}{\partial X^2}\right), \tag{58b}$$

$$M_{XY} = M_{YX} = \int_{-h/2}^{h/2} \tau_{XY} Z dZ = -D(1-\mu)\frac{\partial^2 W}{\partial X \partial Y}. \tag{58c}$$

The axial forces N_X, N_Y and circumferential force S are given by

$$N_X = \int_{-h/2}^{h/2} \sigma_X dZ = \frac{Eh}{1-\mu^2}(\varepsilon_X^m + \mu\varepsilon_Y^m) = h\sigma_X^m, \tag{59a}$$

$$N_Y = \int_{-h/2}^{h/2} \sigma_Y dZ = \frac{Eh}{1-\mu^2}(\varepsilon_Y^m + \mu\varepsilon_X^m) = h\sigma_Y^m, \tag{59b}$$

$$S = \int_{-h/2}^{h/2} \tau_{XY} dZ = \frac{Eh}{1+\mu}\left(\frac{\partial U}{\partial Y} + \frac{\partial V}{\partial X} + \frac{\partial W}{\partial X}\frac{\partial W}{\partial Y}\right) = h\tau_{XY}^m. \tag{59c}$$

In order to keep the plate element in balance, the independent equilibrium equations due to force analysis are given, by neglecting small amount of high orders, in the following forms

$$\sum F_X = 0 \quad \frac{\partial N_X}{\partial X} + \frac{\partial S}{\partial Y} = 0, \tag{60a}$$

$$\sum F_Y = 0 \quad \frac{\partial N_Y}{\partial Y} + \frac{\partial S}{\partial X} = 0, \tag{60b}$$

$$\sum F_Z = 0 \quad \frac{\partial Q_X}{\partial X} + \frac{\partial Q_Y}{\partial Y} + Q + N_X\frac{\partial^2 W}{\partial X^2} + N_Y\frac{\partial^2 W}{\partial Y^2} + 2S\frac{\partial^2 W}{\partial X \partial Y} = 0, \tag{60c}$$

$$\sum M_{YOZ} = 0 \quad \frac{\partial M_Y}{\partial Y} + \frac{\partial M_{XY}}{\partial X} - Q_X = 0, \tag{60d}$$

$$\sum M_{XOZ} = 0 \quad \frac{\partial M_X}{\partial X} + \frac{\partial M_{XY}}{\partial Y} - Q_Y = 0. \tag{60e}$$

Substituting (58a–c) into (60d,e), we obtain the vertical forces Q_X, Q_Y by integration in the following forms

$$Q_X = \int_{-h/2}^{h/2} \tau_{XZ} dZ = -D\frac{\partial}{\partial X}\left(\frac{\partial^2 W}{\partial X^2} + \frac{\partial^2 W}{\partial Y^2}\right), \tag{61a}$$

$$Q_Y = \int_{-h/2}^{h/2} \tau_{YZ} dZ = -D\frac{\partial}{\partial Y}\left(\frac{\partial^2 W}{\partial X^2} + \frac{\partial^2 W}{\partial Y^2}\right). \tag{61b}$$

To make simplification of the original Föppl-von Kármán equations, the Airy function Ψ is introduced satisfying

$$N_X = h\frac{\partial^2 \Psi}{\partial X^2}, \quad N_Y = h\frac{\partial^2 \Psi}{\partial Y^2}, \quad S = -h\frac{\partial^2 \Psi}{\partial X \partial Y}. \tag{62}$$

Substituting (61a,b) and (62) into (60c), (1a) can be obtained. On the other hand, from (59a–c) and (58a–c), we can find forces are only contributed by film stresses which are not related to bending stresses while moments are the opposite. we substitute film stresses expressed by Airy function Ψ into (57a–c) to obtain film strains by combining (59a–c) and (62), then substitute the resulting equations into (56) with consideration of deformation compatibility condition, the full Föppl-von Kármán equations are finally given.

Appendix 2: Symbolic definitions and test functions

Operator $\bullet$ is given in order to emphasize multiplication of tensor matrix with straight vector and matrix $\mathbf{A}$ is a tensor product expressed $\tilde{\mathbf{A}}$. $\hat{\mathbf{G}}$ is straight vector of point value of $G(x, y)$ and elements are coefficients of Coiflets series, which is used to estimate its derivatives vector $\hat{\mathbf{G}}_{u,v}^{d,j}$ by (63) with tensors by resolution Coiflets.

$$\hat{\mathbf{G}}_{u,v}^{d,j} = \left(\widetilde{\Phi}_u^j \bigotimes \widetilde{\Phi}_v^j\right)^T \bullet \hat{\mathbf{G}} \tag{63}$$

where straight vectors of point value and tensors are

$$\widetilde{\Phi}_u^j = \left\{ a_{k,s}^j = \phi_{j,k}^{(u)}\left(\frac{s}{2^j}\right)\right\}, \quad \hat{\mathbf{G}} = \left\{ g_o = G\left(\frac{k}{2^j}, \frac{l}{2^j}\right)\right\},$$
$$\hat{\mathbf{G}}_{u,v}^{d} = \left\{ g_p^d = \frac{\partial^{u+v}}{\partial x^u \partial y^v} G\left(\frac{s}{2^j}, \frac{t}{2^j}\right)\right\},$$
$$o = 2^j k + l + 1,\ p = 2^j s + t + 1, \quad k, l, s, t = 0 \sim 2^j.$$

Definition 1 (**Straight Vector**) If Matrix $\mathbf{A} = \{a_{k,l}\}_{m\times n} \in \mathbb{R}^{m\times n}$, then its horizontal straight vector $\mathfrak{A}$ and vertical straight vector $\check{\mathbf{A}}$ are defined

$$\mathfrak{A} = \{c_r\}_{mn\times 1} \quad a_{k,l} = c_{l+(k-1)m}, \tag{64}$$
$$\check{\mathbf{A}} = \{c_r\}_{mn\times 1} \quad a_{k,l} = c_{k+(l-1)m}. \tag{65}$$

Definition 2 (**Hadamard/Schur Product**) If Matrix $\mathbf{A} = \{a_{k,l}\}_{m\times n}$ and $\mathbf{B} = \{b_{k,l}\}_{m\times n} \in \mathbb{R}^{m\times n}$ (vectors when $m = 1$ and $n = 1$), then their Hadamard/Schur Product $\bigodot$ is defined

$$\mathbf{A} \bigodot \mathbf{B} = \{c_{k,l} = a_{k,l} b_{k,l}\}_{m\times n}. \tag{66}$$

Definition 3 (**Kronecker Tensor Product**) If Matrix $\mathbf{A} = \{a_{k,l}\}_{m\times n}$ and $\mathbf{B} = \{b_{k,l}\}_{p\times q} \in \mathbb{R}^{p\times q}$ (vectors when $m = 1$ and $n = 1$), then their Kronecker Tensor Product $\bigotimes$ is defined

$$\mathbf{A} \bigotimes \mathbf{B} = \{a_{k,l}\mathbf{B}\}_{mp\times nq}. \tag{67}$$

Definition 4 (**Dot Product**) If Matrix $\mathbf{A} = \{a_{k,l}\}_{m\times n} \in \mathbb{R}^{m\times n}$ is a tensor product, as expressed $\tilde{\mathbf{A}}$. $\hat{\mathbf{B}} = \{b_k\}_{n\times 1} \in \mathbb{R}^{n\times 1}$ is straight vector of matrix $\mathbf{B} = \{b_{k,l}\}_{p\times q} \in \mathbb{R}^{p\times q}$ while $n = pq$, then their matrix product $\bullet$ is emphasized

$$\tilde{\mathbf{A}} \bullet \hat{\mathbf{B}} = \{a_{k,l} b_k\}_{m\times 1}. \tag{68}$$

In linear cases, test Function $T(x, y)$ with exact solution $U(x, y)$

$$\begin{aligned} T(x,y) = 294912\big[&x^6(5y^2-5y+1) - 3x^5(5y^2-5y+1) \\ &+ x^4(25y^4-50y^3+45y^2-20y+3) \\ &+ x^3(-50y^4+100y^3-65y^2+15y-1) \\ &+ x^2y(5y^5-15y^4+45y^3-65y^2+36y-6) \\ &+ x(-5y^6+15y^5-20y^4+15y^3-6y^2+y) + (y-1)^3y^3\big]. \\ U(x,y) = 2^{12}&(1-x)^3x^3(1-y)^3y^3. \end{aligned} \tag{69}$$

In nonlinear validation case, for simply supported boundary

$$\begin{aligned} q_1(x,y) = \frac{1}{8}\big[&-9\pi^4\cos(\pi x+\pi y) + 25\pi^4\cos(3\pi x+\pi y) \\ &- 100\pi^4\cos(\pi x+2\pi y) + 25\pi^4\cos(\pi x+3\pi y) \\ &- 9\pi^4\cos(3\pi x+3\pi y) - 9\pi^4\cos(\pi x-\pi y) \\ &+ 25\pi^4\cos(3\pi x-\pi y) + 100\pi^4\cos(\pi x-2\pi y) \\ &+ 25\pi^4\cos(\pi x-3\pi y) - 9\pi^4\cos(3\pi x-3\pi y)\big]. \end{aligned} \tag{70}$$

$$\begin{aligned} p_1(x,y) = \frac{1}{50}\big[&625\pi^4\cos(2\pi x+\pi y) + 625\pi^4\cos(2\pi x-\pi y) \\ &- 9\pi^4\cos(2\pi x) - 9\pi^4\cos(4\pi y)\big] \end{aligned} \tag{71}$$

with the analytical solutions

$$w_1(x,y) = \sin(2\pi x)\sin(\pi y), \quad \varphi_1(x,y) = \sin(\pi x)\sin(2\pi y). \tag{72}$$

For circled clamped boundary

$$\begin{aligned} q_2(x,y) = &2\pi^4\cos(\pi x+2\pi y) - 3\pi^4\cos(3\pi x+2\pi y) \\ &+ 50\pi^4\cos(2\pi x+4\pi y) - 3\pi^4\cos(\pi x+6\pi y) \\ &- 2\pi^4\cos(\pi x-2\pi y) + 3\pi^4\cos(3\pi x-2\pi y) \\ &+ 50\pi^4\cos(2\pi x-4\pi y) + 3\pi^4\cos(\pi x-6\pi y) \\ &- 4\pi^4\cos(2\pi x) - 64\pi^4\cos(4\pi y), \end{aligned} \tag{73}$$

$$\begin{aligned} p_2(x,y) = \frac{1}{100}\big[&-1250\pi^4\cos(\pi x+2\pi y) + 18\pi^4\cos(2\pi x+4\pi y) \\ &- 9\pi^4\cos(4\pi x+4\pi y) - 9\pi^4\cos(2\pi x+8\pi y) \\ &+ 1250\pi^4\cos(\pi x-2\pi y) + 18\pi^4\cos(2\pi x-4\pi y) \\ &- 9\pi^4\cos(4\pi x-4\pi y) - 9\pi^4\cos(2\pi x-8\pi y) \\ &- 18\pi^4\cos(2\pi x) + 18\pi^4\cos(4\pi x) \\ &- 18\pi^4\cos(4\pi y) + 18\pi^4\cos(8\pi y)\big]. \end{aligned} \tag{74}$$

with the analytical solutions

$$w_2(x,y) = \frac{1}{4}(1-\cos 2\pi x)(1-\cos 4\pi y), \quad \varphi_2(x,y) = \sin(\pi x)\sin(2\pi y). \tag{75}$$

and combined boundary corresponding to

$$\begin{aligned} q_3(x,y) = \frac{1}{16}\big[& -11\pi^4\sin(\pi x+\pi y) - 100\pi^4\sin(2\pi x+\pi y) \\ & + 25\pi^4\sin(3\pi x+\pi y) + 27\pi^4\sin(\pi x+3\pi y) \\ & - 9\pi^4\sin(3\pi x+3\pi y) - 11\pi^4\sin(\pi x-\pi y) \\ & + 100\pi^4\sin(2\pi x-\pi y) + 25\pi^4\sin(3\pi x-\pi y) \\ & + 27\pi^4\sin(\pi x-3\pi y) - 9\pi^4\sin(3\pi x-3\pi y) \\ & + 8\pi^4\sin(\pi y)\big], \end{aligned} \tag{76}$$

$$\begin{aligned} p_3(x,y) = \frac{1}{400}\big[& -5000\pi^4\cos(\pi x+2\pi y) + 9\pi^4\cos(2\pi x+2\pi y) \\ & + 5000\pi^4\cos(\pi x-2\pi y) + 9\pi^4\cos(2\pi x-2\pi y) \\ & - 18\pi^4\cos(2\pi x) + 18\pi^4\cos(4\pi x) - 18\pi^4\cos(2\pi y)\big] \end{aligned} \tag{77}$$

with the analytical solutions

$$w_3(x,y) = \frac{1}{2}(1-\cos 2\pi x)\sin(\pi y), \quad \varphi_3(x,y) = \sin(\pi x)\sin(2\pi y). \tag{78}$$

References

1. Föppl, A.: Vorlesungen über technische mechanik Bd. 3,B.G. Teubner, Leipzig (1907)
2. von Karman, T.: Festigkeitsproblem im maschinenbau. Encyk. D. Math. Wiss. **4**, 311–385 (1910)
3. Sokolnikoff, I.S.: Mathematical Theory of Elasticity. McGraw-Hill (1956)
4. Landau, L.D., Lifshit'S, E.M..: Theory of Elasticity. World Book Publishing Company (1999)
5. Knightly, G.H.: An existence theorem for the von Kármán equations. Arch. Ration. Mech. Anal. **27**(3), 233–242 (1967)
6. Kesavan, S.: Application of Kikuchi's method to the von Kármán equations. Numer. Math. **32**(2), 209–232 (1979)
7. Chueshov, I.D.: On the finiteness of the number of determining elements for von Kármán evolution equations. Math. Methods Appl. Sci. **20**(10), 855–865 (1997)
8. da Silva, P.P., Krauth, W.: Numerical solutions of the von Kármán equations for a thin plate. Int. J. Modern Phys. C **8**(2), 427–434 (1996)
9. Lewicka, M., Mahadevan, L., Pakzad, M.R.: The föppl-von Kármán equations for plates with incompatible strains. Proc. R. Soc. Lond. **467**(2126), 402–426 (2011)
10. Xue, C.X., Pan, E., Zhang, S.Y., Chu, H.J.: Large deflection of a rectangular magnetoelectroelastic thin plate. Mech. Res. Commun. **38**(7), 518–523 (2011)
11. Ciarlet, G.P., Gratie, L., Kesavan, S.: Numerical analysis of the generalized von Kármán equations. Comptes Rendus Mathematique **341**(11), 695–699 (2005)
12. Ciarlet, P.G., Gratie, L., Kesavan, S.: On the generalized von Kármán equations and their approximation. Math. Models Methods Appl. Sci. **17**(04), 617–633 (2007)
13. Ciarlet, P.G., Gratie, L.: From the classical to the generalized von Kármán and marguerre–von Kármán equations. J. Comput. Appl. Math. **190**(1-2), 470–486 (2006)
14. Ciarlet, P.G., Paumier, J.C.: A justification of the marguerre-von Kármán equations. Comput. Mech. **1**(3), 177–202 (1986)
15. Ciarlet, P.G., Gratie, L., Sabu, N.: An existence theorem for generalized von Kármán equations. J. Elast. **62**(3), 239–248 (2001)
16. Milani, A.J., Chueshov, I., Lasiecka, I.: Von Kármán Evolution Equations. Springer, New York (2010)
17. Coman, C.D.: On the compatibility relation for the föppl-von Kármán plate equations. Appl. Math. Lett. **25**(12), 2407–2410 (2012)

18. Doussouki, A.E., Guedda, M., Jazar, M., Benlahsen, M.: Some remarks on radial solutions of föppl-von Kármán equations. Appl. Math. Comput. **219**(9), 4340–4345 (2013)
19. Van Gorder, R.A.: Analytical method for the construction of solutions to the föppl-von kármán equations governing deflections of a thin flat plate. Int. J. Non-Linear Mech. **47**(3), 1–6 (2012)
20. Liao, S.J.: The proposed homotopy analysis technique for the solution of nonlinear problems. Shanghai Jiao Tong University, Ph.d thesis (1992)
21. Liao, S.J.: Notes on the homotopy analysis method: some definitions and theorems. Commun. Nonlinear Sci. Numer. Simul. **14**(4), 983–997 (2009)
22. Zou, K., Nagarajaiah, S.: An analytical method for analyzing symmetry-breaking bifurcation and period-doubling bifurcation. Commun. Nonlinear Sci. Numer. Simul. **22**(1–3), 780–792 (2014)
23. Van Gorder, R.A., Vajravelu, K.: Analytic and numerical solutions to the laneemden equation. Phys. Lett. A **372**(39), 6060–6065 (2008)
24. Varol, Y., Oztop, H.F.: Control of buoyancy-induced temperature and flow fields with an embedded adiabatic thin plate in porous triangular cavities. Appl. Therm. Eng. **29**(2–3), 558–566 (2009)
25. Mastroberardino, A.: Homotopy analysis method applied to electrohydrodynamic flow. Commun. Nonlinear Sci. Numer. Simul. **16**(7), 2730–2736 (2011)
26. Van Gorder, R.A.: Relation between laneemden solutions and radial solutions to the elliptic heavenly equation on a disk. New Astron. **37**, 42–47 (2015)
27. Ablowitz, M.J., Ladik, J.F.: Nonlinear differential–difference equations and fourier analysis. J. Math. Phys. **17**(6), 1011–1018 (1976)
28. Stein, E.M., Weiss, G.: Introduction to fourier analysis on euclidean spaces. Princeton Math. Ser. **212**(2), 484–503 (2009)
29. Wang, J.Z.: Generalized theory and arithmetic of orthogonal wavelets and applications to researches of mechanics including piezoelectric smart structures. Lanzhou University, Ph.d thesis (2001)
30. Zhou, Y.H., Wang, J.Z.: Generalized gaussian integral method for calculations of scaling function transform of wavelets and its applications. Acta Mathematica Scientia(Chinese Edition) **19**(3), 293–300 (1999)
31. Chen, M.Q., Hwang, C., Shih, Y.P.: The computation of wavelet-galerkin approximation on a bounded interval. Int. J. Numer. Methods Eng. **39**(17), 2921–2944 (1996)
32. Xing, R.: Wavelet-based homotopy analysis method for nonlinear matrix system and its application in burgers equation. Math. Problems Eng. 2013,(2013-6-25) **2013**(5), 14–26 (2013)
33. Muskhelishvili, N.I.: Some Basic Problems of the Mathematical Theory of Elasticity. P.Noordhoff Ltd (1953)
34. Tian, J.: The Mathematical Theory and Applications of Biorthogonal Coifman Wavelet Systems. Rice University, Ph.D. thesis (1996)
35. Liu, X.J.: A Wavelet Method for Uniformly Solving Nonlinear Problems and Its Application to Quantitative Research on Flexible Structures with Large Deformation. Lanzhou University, Ph.d thesis (2014)
36. Katsikadelis, J.T., Nerantzaki, M.S.: Non-linear analysis of plates by the analog equation method. Comput. Mech. **14**(2), 154–164 (1994)
37. Azizian, Z.G., Dawe, D.J.: Geometrically nonlinear analysis of rectangular mindlin plates using the finite strip method. Comput. Struct. **21**(3), 423–436 (1985)
38. Wang, W., Ji, X., Tanaka, M.: A dual reciprocity boundary element approach for the problems of large deflection of thin elastic plates. Comput. Mech. **26**(1), 58–65 (2000)
39. Al-Tholaia, M.M.H., Al-Gahtani, H.J.: Rbf-based meshless method for large deflection of elastic thin plates on nonlinear foundations. Eng. Anal. Bound. Elements **51**, 146–155 (2015)
40. Zhao, Y., Lin, Z., Liao, S.: An iterative ham approach for nonlinear boundary value problems in a semi-infinite domain. Comput. Phys. Commun. **184**(9), 2136–2144 (2013)
41. Katsikadelis, J.T.: Large deflection analysis of plates on elastic foundation by the boundary element method. Int. J. Solids Struct. **27**(15), 1867–1878 (1991)